Journal of Molecular Liquids 363 (2022) 119844

Contents lists available at ScienceDirect

Journal of Molecular Liquids

journal homepage: www.elsevier.com/locate/molliq

Effect of a confining surface on a mixture with spontaneous inhomogeneities

O. Patsahan [a], A. Meyra [b,c], A. Ciach [d,*]

[a] Institute for Condensed Matter Physics of the National Academy of Sciences of Ukraine, 1 Svientsitskii St., 79011 Lviv, Ukraine
[b] Instituto de Física de Líquidos y Sistemas Bilógicos, UNLP-CONICET, 59-789, 1900 La Plata, Argentina
[c] Depto. Ing. Mecánica 60 124, UTN-FRLP, 1900 La Plata, Argentina
[d] Institute of Physical Chemistry, Polish Academy of Sciences, 01-224 Warszawa, Poland

ARTICLE INFO

Article history:
Received 7 May 2022
Revised 11 July 2022
Accepted 12 July 2022
Available online 16 July 2022

Keywords:
Complex mixture
Self-assembly
Effect of clustering on adsorption
Theory for mesoscopic inhomogeneities

ABSTRACT

A binary self-assembling mixture near a planar wall is studied by theory and Monte Carlo simulations. The grand potential functional of the local concentration and the local volume fraction of all particles is developed in the framework of the density functional and field-theoretic methods. We obtain ordinary differential Euler–Lagrange equations for the concentration and the volume fraction, and solve them analytically in the perturbation expansion. The obtained exponentially damped oscillations of the concentration, with the characteristic lengths the same as in the concentration-concentration correlation function, agree very well with simulations. For the excess volume fraction we obtain a monotonic decay superimposed on the exponentially damped oscillations with a fair agreement with simulations. The period of the density oscillations is equal to half the period of the concentration oscillations in both the theory and simulations. Simulations show local ordering in the layers parallel to the wall that are rich in one of the two components. Bubbles, stripes and clusters appear in the subsequent layers for increasing distance from the wall. Between these almost one-component layers the density takes minima, and a bulk-like structure with clusters of different particles being nearest neighbors appears.

1. Introduction

Biological and soft-matter systems are strongly inhomogeneous, and the effect of boundaries in their case is significantly different than in simple fluids. In the case of systems with spontaneous inhomogeneities, confinement in regions of various sizes and shapes leads to significant structural modifications resulting in changes of thermodynamic and mechanical properties. These effects have been studied over decades [1–14]. In contrast, adsorption phenomena in systems with spontaneous inhomogeneities attracted much less attention [7–9], despite the fact that surfaces of different kind play a very important role in biological and soft-matter systems. In this work, we address the general question of the effect of a planar wall on a mixture with spontaneous inhomogeneities that occur on a mesoscopic length scale.

In biological and soft-matter systems, the interactions or effective interactions between particles can be quite complex, and often exhibit competing tendencies. A representative example is the short-range attraction long-range repulsion (SALR) between charged particles or globular proteins in complex solvents inducing the short-range attraction. When the particles interact with the SALR potential, stable clusters can be formed when a density of a dilute system increases, and/or temperature decreases [15]. The onset of clustering can be identified with the appearance of a maximum at $n = n_o > 1$ of the probability $P(n)$ that a randomly chosen particle is a member of a cluster consisting of n particles [16]. $P(n_o)$ increases with increasing density of the particles, and becomes equal to $P(1)$ at the crossover between monomer- and cluster dominated system. At this crossover, the specific heat takes a maximum, since the energy fluctuations are large when clusters assemble and disassemble with a high probability [8].

In the monomer dominated system, the adsorption at an attractive surface at $z = 0$ has the same qualitative behavior as in simple fluids. Namely, the adsorption $\Gamma = \int_0^\infty dz(\zeta(z) - \zeta_b)$, where $\zeta(z)$ and ζ_b are the volume fraction at the distance z from the wall and in the bulk, respectively, increases with increasing chemical potential μ [9]. At the crossover between the monomer- and cluster dominated systems, however, $\Gamma(\mu)$ takes a maximum [9]. Further increase of μ leads to decreasing Γ, which means that new particles introduced to the system are not adsorbed at the surface, but remain in the bulk. This is because the sum of the interactions

* Corresponding author.
E-mail address: alina.ciach@gmail.com (A. Ciach).

https://doi.org/10.1016/j.molliq.2022.119844
0167-7322/

of a particle in the bulk with all the adsorbed clusters is strongly repulsive. The repulsion keeps the particle away from the surface, and leads to a broad depletion zone after the adsorbed layer of clusters [8]. As shown by simulations, the excess density exhibits an oscillatory decay, $\zeta(z)-\zeta_b \propto \exp(-\alpha_0 z)\sin(\alpha_1 z+\theta)$, with the period $2\pi/\alpha_1$ and the decay length $1/\alpha_0$ the same as in the bulk correlation function [8]. This asymptotic behavior of $\zeta(z)-\zeta_b$ predicted theoretically for $z\to\infty$ [17] agrees very well with simulations for z just after the depletion zone [8]. It is worth mentioning that the decay of the charge density in ionic liquids near an electrode follows the same asymptotic behavior already for $z>2\pi/\alpha_1$ as well [18].

Another interesting property distinguishing the SALR system from simple fluids is the structure near a hard wall. A particle at the wall interacts with the fluid particles, and this interaction is not compensated by the interaction with the missing particles at $z<0$. In simple fluids, the particle at the wall is pulled to the bulk, because of the uncompensated attraction by the fluid particles. In the SALR system, however, the long-range repulsion by the fluid particles is not compensated, and particles near the wall are pushed towards it. Such an effective attraction by the hard wall was observed in simulations and in DFT calculations [12,13,11,14]. The strength of the effect of the missing neighbors was predicted in [17] in the mean-field (MF) approximation.

A very powerful method of determining the structure near solid surfaces or at interfaces, is the classical density functional theory (DFT) [19,20]. It gives accurate predictions for the density profiles near the surface. Minimization of the functional, especially for complex systems, is not trivial, however. The Euler–Lagrange (EL) equations are very complex, and can be solved only numerically at rather large computational cost. Finally, the results are limited to particular examples. The EL equations in the phenomenological Landau theory, where the interactions with the wall and the compensation for the missing neighbors are taken into account in a simple surface contribution to the Landau functional, are much simpler [21]. The ordinary differential EL equations can be solved analytically, but the results are only qualitative and are given in terms of phenomenological parameters. The advantage is a general overview of possible types of solutions of the EL equations for a broad range of phenomenological parameters, but a microscopic theory or experimental results are necessary for determining the values of the phenomenological parameters for particular systems.

A compromise between the DFT and the Landau-type theory is the mesoscopic theory developed for the semiinfinite SALR system in Ref.[17]. In this theory, the grand-potential functional is coarse-grained and transformed to a functional that has the Landau-type form, but all parameters are given in terms of interactions and thermodynamic variables. The missing-neighbors contribution is given in terms of odd semi-moments of the interaction potential. The theory, however, is of the MF type, whereas in inhomogeneous systems fluctuations of the local density, i.e. in fact formation of clusters or depleted regions between them, play an essential role.

Biological and soft-matter systems are typically inhomogeneous and multicomponent, but mixtures with competing interactions did not attract much attention until very recently [22–26]. Addition of a second component to particles interacting with the SALR potential can lead to formation of different aggregates, depending on the interactions between the second-component particles and on the cross-interaction. The cross-interaction may have different forms, depending on the nature of the particles and of the solvent. Depending on the strength of the cross-interaction, giant clusters with mixed or separated components, or chains of alternating clusters of different species were observed in simulations of a binary mixture with the SALR interactions between all the pairs of the particles [23]. In another, experimentally relevant example, for the cross-interaction a repulsion at short- and an attraction at large distances was assumed in the simulation and theoretical studies [24,25]. Oppositely charged solvophilic and solvophobic particles attract each other at large distances, and repel each other at shorter distances due to the thermodynamic Casimir potential when the solvent approaches its critical point [27–29]. The Casimir potential between like particles is attractive, therefore like charged particles interact with the SALR potential. The Casimir potential can be tuned by controlling the temperature. In simulation and theoretical studies of such a mixture with interactions favoring small clusters of like particles, a coexistence of a gas and a dense phase with alternating bilayers of the two components was observed for equal numbers of particles of the two components. In the disordered phase, the correlation function for the concentration fluctuations exhibits exponentially damped oscillations, and the period of the oscillations can be tuned by changing the shape of the potential [25,24].

In general, in one component systems either macroscopic gas–liquid transition, or alternating mesoscopic dense and dilute domains can be formed. The density waves in different directions can interfere leading to phases with different symmetry [30]. In binary mixtures, we can have demixing on the macroscopic or mesoscopic length scale in addition to the separation into dense and dilute regions [31]. Interference of the density and concentration waves can produce more complex structures. The types of aggregates for different concentrations and densities and the whole phase diagrams for binary mixtures with competing interactions are not known yet.

Because of many open questions concerning the bulk properties of mixtures with competing interactions, the effect of confinement on such mixtures has not attracted much attention yet. However, as shown by molecular dynamics simulations in Ref.[7], nontrivial adsorption phenomena can occur at a planar surface for the system with the phase diagram determined in Ref.[24]. When the gas phase in the bulk is close to the coexistence with the dense ordered phase, very interesting structural changes occur at a selective surface attracting only the first component. When the wall-particle attraction is moderate, a dense and quite thick film with the alternating bilayers perpendicular to the wall is adsorbed. When the wall-particle attraction becomes very strong, the alternating layers are parallel to the surface, and ordered internal patterns in the layers at some distance from the wall develop.

As far as we know, no theoretical predictions for the effect of a wall on the disordered inhomogeneous mixture have been published so far. In this work, a mesoscopic theory for binary mixtures near a planar wall is developed. We take into account fluctuations of the local densities by combining the DFT and field-theoretic methods. Our theory for the bulk is summarized in Section 2. We focus on symmetrical binary mixtures, such as those studied in Ref.[24,25], and obtain the grand potential functional for a semiinfinite system in Section 3. In Section 3.1, the derivation of the functional is presented. Explicit expressions for the EL equations for the volume fraction and concentration, and the boundary conditions are developed in Section 3.2. We solve the equations analytically in a perturbation expansion in Section 3.3. In Section 4 a particular model for the symmetrical binary mixture is considered. We obtain the correlation functions and the concentration and density profiles from our analytical expressions in Section 4.1. Our results are compared with Monte Carlo (MC) simulations in Section 4.2. Section 5 contains our conclusions.

2. Mesoscopic theory for inhomogeneous binary mixtures

In this section we briefly summarize the formalism allowing for addition of terms depending on the variance of local densities to

the grand potential density functional [31,24]. Next, we develop approximate equations for the correlation functions in the case of symmetrical binary mixtures. In our theory, the methods of the DFT are combined with an extension of the Brazovskii field theory [32].

In order to describe the structure on the mesoscopic length scale, we consider the volume fraction $\zeta_i(\mathbf{r})$ of the i-th component in the mesoscopic region around $\mathbf{r}$, and external fields $h_i(\mathbf{r})$ acting on the i-th component, varying on the mesoscopic length scale as well. We consider a binary mixture with $i = 1, 2$, but generalization to more components is straightforward. The generating functional for the correlation functions is $-\beta\Omega_h[\{h_i\}]$, where

$$\beta\Omega_h[\{h_i\}] = -\ln \int D\zeta_1 \int D\zeta_2 \exp\left(-\beta\Omega_{co}[\{\zeta_i\}] + \int d\mathbf{r}\beta h_i(\mathbf{r})\zeta_i(\mathbf{r})\right) \quad (1)$$

is the grand potential in a presence of the external fields $h_i(\mathbf{r})$ in $k_BT = 1/\beta$ units, with k_B and T denoting the Boltzmann constant and temperature, respectively. In (1) and below the summation convention for repeated indexes is used. Note that in (1) we have the factor $\exp[-\beta\Omega_{co}]$ instead of the Boltzmann factor $\exp(-\beta H)$, where H is the microscopic Hamiltonian. Moreover, the functional integrals are over the mesoscopic volume fractions ζ_i, rather than over all microscopic states. This is because in (1) the integration over the mesoscopic degrees of freedom, ζ_i, and the integration over the microscopic states for each fixed ζ_i are performed separately. The integration of the Boltzmann factor $\exp(-\beta H)$ over the microscopic states for given ζ_i leads to the factor $\exp[-\beta\Omega_{co}]$, where Ω_{co} is the grand potential for the system with suppressed fluctuations around $\zeta_i(\mathbf{r})$.

The average mesoscopic volume fraction at $\mathbf{r}$, and the correlation function between fluctuations of ζ_i in the mesoscopic regions around $\mathbf{r}_1$ and $\mathbf{r}_2$ are given by

$$\bar{\zeta}_i(\mathbf{r}) = \frac{\delta(-\beta\Omega_h)}{\delta(\beta h_i(\mathbf{r}))} \quad (2)$$

and

$$G_{ij}(\mathbf{r}_1 - \mathbf{r}_2) = \langle\zeta_i(\mathbf{r}_1)\zeta_j(\mathbf{r}_2)\rangle - \bar{\zeta}_i(\mathbf{r}_1)\bar{\zeta}_j(\mathbf{r}_2) = \frac{\delta\bar{\zeta}_i(\mathbf{r}_1)}{\delta\beta h_j(\mathbf{r}_2)}. \quad (3)$$

The Legendre transform

$$\beta\Omega[\{\bar{\zeta}_i\}] = \beta\Omega_h[\{h_i\}] + \int d\mathbf{r}\beta h_i(\mathbf{r})\bar{\zeta}_i(\mathbf{r}) \quad (4)$$

is a functional of $\bar{\zeta}_i$, generating the inverse correlation functions,

$$C_{ij}(\mathbf{r}_1 - \mathbf{r}_2) = \frac{\delta^2\beta\Omega}{\delta\bar{\zeta}_i(\mathbf{r}_1)\delta\bar{\zeta}_j(\mathbf{r}_2)} = \frac{\delta\beta h_i(\mathbf{r}_1)}{\delta\bar{\zeta}_j(\mathbf{r}_2)}. \quad (5)$$

From (3) and (5) one can easily get the analog of the Ornstein–Zernike (OZ) equation relating the correlation and the inverse (in the matrix sense) correlation functions, $\mathbf{G}$ and $\mathbf{C}$, with the elements G_{ij} and C_{ij}, respectively,

$$\int d\mathbf{r}_3 C_{ij}(\mathbf{r}_1 - \mathbf{r}_3)G_{jk}(\mathbf{r}_3 - \mathbf{r}_2) = \delta(\mathbf{r}_1 - \mathbf{r}_2)\delta^{Kr}_{ik}. \quad (6)$$

Using (1), we rewrite (4) in the form

$$\beta\Omega[\{\bar{\zeta}_i\}] = \beta\Omega_{co}[\{\bar{\zeta}_i\}] - \ln \int D\phi_1 \int D\phi_2 \exp\left(-\beta H_f[\{\bar{\zeta}_i, \phi_i\}]\right) \quad (7)$$

where $\phi_i(\mathbf{r}) = \zeta_i(\mathbf{r}) - \bar{\zeta}_i$ is the local fluctuation of ζ_i, and

$$\beta H_f[\{\bar{\zeta}_i, \phi_i\}] = \beta\Omega_{co}[\{\bar{\zeta}_i + \phi_i\}] - \beta\Omega_{co}[\{\bar{\zeta}_i\}] - \int d\mathbf{r}\beta h_i(\mathbf{r})\phi_i(\mathbf{r}). \quad (8)$$

In the disordered phase with $h_i = 0, \bar{\zeta}_i$ does not depend on the position.

From (5) and (7) we can see that the matrix $\mathbf{C}$ contains a contribution from $\beta\Omega_{co}$ associated with microscopic fluctuations (the first term in (7)), and the contribution associated with the mesoscopic fluctuations $\phi_i(\mathbf{r})$ (the second term in (7)). The fluctuations of the local densities play important role in systems with spontaneous inhomogeneity, since the density inside the clusters is larger than between them, and the clusters move freely in the disordered phase. In the course of time, the clusters enter or leave the mesoscopic subsystem at $\mathbf{r}$, therefore local deviations from $\bar{\zeta}_i$ appear with a large probability, leading to a large fluctuation contribution to the grand potential. The separation of the microscale from the mesoscale fluctuations allows us to use the methods of the field theory in calculations of the correlation functions at large separations.

In order to proceed, we need to know the form of Ω_{co} that should satisfy the general thermodynamic formula

$$\Omega_{co}[\{\zeta_i\}] = U_{co}[\{\zeta_i\}] - TS_{co}[\{\zeta_i\}] - \mu_i \int d\mathbf{r}\zeta_i(\mathbf{r}). \quad (9)$$

$U_{co}[\{\zeta_i\}]$ and $S_{co}[\{\zeta_i\}]$ are the internal energy and the entropy, respectively, in the presence of the constraints $\{\zeta_i\}$ imposed on the microscopic states, and μ_i is the chemical potential of the i-th species. Exact determination of U_{co} and S_{co} is a very difficult task. However, in the case of suppressed mesoscopic fluctuations, these quantities can be approximated by the well-known MF formulas. We make the approximation

$$U_{co}[\{\zeta_i\}] = \frac{1}{2}\int d\mathbf{r}_1 \int d\mathbf{r}\zeta_i(\mathbf{r}_1)V_{ij}(r)\zeta_j(\mathbf{r}_1 + \mathbf{r}), \quad (10)$$

where $r = |\mathbf{r}|$. By $V_{ij}(r)$ we denote the product of the interaction between particles of the i-th and j-th component and the pair distribution function $g_{ij}(r)$. For the system with suppressed mesoscopic fluctuations we assume $g_{ij}(r) = \theta\big(r - (\sigma_i + \sigma_j)/2\big)$, where σ_i is the diameter of the i-th species and θ is the unit step function. With this assumption, we avoid contributions to the energy from overlapping hard cores of the particles. Because in (9) and (10) we use $\zeta_i = \pi\rho_i/6$, where ρ_i is the dimensionless density, μ_i and $V_{ij}(r)$ should be in appropriate units. Finally, we assume $-TS_{co} = \int d\mathbf{r} f_h(\zeta_1(\mathbf{r}), \zeta_2(\mathbf{r}))$, where

$$\beta f_h = \rho_1 \ln\rho_1 + \rho_2 \ln\rho_2 + \beta f_{ex} \quad (11)$$

is the free-energy per unit volume of the hard-core reference system in the local-density approximation. The first two terms come from the entropy of mixing, and the last term describes packing of hard cores. For the latter term, the Carnahan-Starling (CS) approximation [33] can be used.

The rather difficult problem of calculating the correlation functions from (5)–(8) simplifies greatly in symmetrical mixtures with $\mu_1 = \mu_2$, and $V_{ii} = -V_{ij} = V$ (see [24,25]). The above property has for example the restricted primitive model (RPM) for ions or particles with the positive and negative charge of the same magnitude and with the spherical hard cores of the same size. From now on we limit ourselves to such symmetrical mixtures. In the symmetrical case, it is convenient to consider the total volume fraction and the concentration, $\zeta = \zeta_1 + \zeta_2$ and $c = \zeta_1 - \zeta_2$, respectively, because in the absence of external fields $\bar{c} = 0$ by symmetry. Moreover, in these variables the internal energy (10) takes the simple form

$$\begin{aligned} U_{co} &= \frac{1}{2}\int d\mathbf{r}_1 \int d\mathbf{r} c(\mathbf{r}_1)V(r)c(\mathbf{r}_1 + \mathbf{r}) \\ &= \frac{1}{2}\int d\mathbf{k}\hat{c}(\mathbf{k})\hat{V}(k)\hat{c}(-\mathbf{k}), \end{aligned} \quad (12)$$

where $\hat{V}(k)$ and $\hat{c}(\mathbf{k})$ denote the functions V and c in Fourier representation, and $k = |\mathbf{k}|$. We will use the same convention (a hat) for all functions in Fourier representation in the 3 dimensional space.

We shall calculate the correlation functions for the fields c and ζ, $G_{cc}(r)=\langle c(\mathbf{r}_1)c(\mathbf{r}_1+\mathbf{r})\rangle$ and $G_{\zeta\zeta}(r)=\langle\zeta(\mathbf{r}_1)\zeta(\mathbf{r}_1+\mathbf{r})\rangle-\bar{\zeta}^2$. For the inverse correlation functions we obtain, using (7) the following expression

$$C_{\alpha\beta}(r)=\frac{\delta^2\beta\Omega}{\delta\alpha(\mathbf{r}_1)\delta\beta(\mathbf{r}_1+\mathbf{r})}=\frac{\delta^2(\beta\Omega_{co})}{\delta\alpha(\mathbf{r}_1)\delta\beta(\mathbf{r}_1+\mathbf{r})}+\left\langle\frac{\delta^2(\beta H_f)}{\delta\alpha(\mathbf{r}_1)\delta\beta(\mathbf{r}_1+\mathbf{r})}-\frac{\delta(\beta H_f)}{\delta\alpha(\mathbf{r}_1)}\frac{\delta(\beta H_f)}{\delta\beta(\mathbf{r}_1+\mathbf{r})}\right\rangle \tag{13}$$

where $\alpha=c,\zeta,\beta=c,\zeta$.

Note that

$$A_{m,n}(c,\zeta)=\frac{\partial^{n+m}(\beta f_h)}{\partial^n c\partial^m\zeta} \tag{14}$$

has the property $A_{m,2n+1}(0,\bar{\zeta})=0$, because derivatives of an even function of c vanish at $c=0$. As a result $C_{\zeta c}=0$, and the fields c and ζ are the eigenvectors of the matrices $\mathbf{C}$ and $\mathbf{G}=\mathbf{C}^{-1}$, therefore the correlation functions $G_{cc}(r)$ and $G_{\zeta\zeta}(r)$ in Fourier representation are simply given by

$$\hat{G}_{\alpha\alpha}(k)=1/\hat{C}_{\alpha\alpha}(k). \tag{15}$$

The probability that a local fluctuation $\phi=c-\bar{c},\psi=\zeta-\bar{\zeta}$ appears, is proportional to $\exp(-\beta H_f)$, and the correlation functions can be obtained from the formula

$$G_{cc}(\mathbf{r}_1,\mathbf{r}_2)=\langle\phi(\mathbf{r}_1)\phi(\mathbf{r}_2)\rangle=\frac{\int D\phi\int D\psi e^{-\beta H_f}\phi(\mathbf{r}_1)\phi(\mathbf{r}_2)}{\int D\phi\int D\psi e^{-\beta H_f}}, \tag{16}$$

with analogous expression for $G_{\zeta\zeta}$. We make the approximation

$$\beta H_f[\{\bar{\zeta}_i,\phi_i\}]\approx\beta H_G[\bar{c},\bar{\zeta},\phi,\psi] \tag{17}$$

with

$$\beta H_G[\bar{c},\bar{\zeta},\phi,\psi]=\frac{1}{2}\int d\mathbf{r}_1\int d\mathbf{r}_2(\phi(\mathbf{r}_1)C_{cc}(r)\phi(\mathbf{r}_2)+\psi(\mathbf{r}_1)C_{\zeta\zeta}(r)\psi(\mathbf{r}_2)+2\phi(\mathbf{r}_1)C_{c\zeta}(r)\psi(\mathbf{r}_2)), \tag{18}$$

where $C_{\alpha\beta}$ is a functional of $\bar{c},\bar{\zeta}$ satisfying (13). Because $C_{c\zeta}=0$ for $\bar{c}=0$ (vanishing external fields), we obtain in Fourier representation $\hat{G}_{cc}(k)=1/\hat{C}_{cc}(k)$ for G_{cc} defined in (16), and $\hat{G}_{\zeta\zeta}(k)=1/\hat{C}_{\zeta\zeta}(k)$ for $G_{\zeta\zeta}$ defined by an equation analogous to (16). Thus, when H_f is approximated by (17) and (18), $C_{\alpha\alpha}$ can be obtained for $\bar{c}=0$ by a self-consistent solution of (13).

In order to solve self-consistently Eqs. (13)–(18), we assume that the fluctuation contribution to the two-point functions should be taken into account according to Eq. (13), but for the higher-order functional derivatives of $\beta\Omega$ (i.e. the functional derivatives of $C_{\alpha\beta}$), the fluctuation contribution in (7) can be disregarded. This approximation for $C_{\alpha\beta}$ corresponds to the self-consistent one-loop approximation in the field-theoretic approach. Based on this assumption, we make for $n+m>2$ the approximation

$$\frac{\delta^{n+m}(\beta\Omega)}{\delta c(\mathbf{r}_1)\dots\delta c(\mathbf{r}_n)\delta\zeta(\mathbf{r}_{n+1})\dots\delta\zeta(\mathbf{r}_{n+m})}\approx\frac{\delta^{n+m}(\beta\Omega_{co})}{\delta c(\mathbf{r}_1)\dots\delta c(\mathbf{r}_n)\delta\zeta(\mathbf{r}_{n+1})\dots\delta\zeta(\mathbf{r}_{n+m})}. \tag{19}$$

In the local density approximation for $\beta f_h(\{\zeta_i\})$, we have for $n+m>2$

$$\frac{\delta^{n+m}(\beta\Omega_{co})}{\delta c(\mathbf{r}_1)\dots\delta c(\mathbf{r}_n)\delta\zeta(\mathbf{r}_{n+1})\dots\delta\zeta(\mathbf{r}_{n+m})}=A_{m,n}(c,\zeta)\delta(\mathbf{r}_1-\mathbf{r}_2)\dots\delta(\mathbf{r}_{n+m-1}-\mathbf{r}_{m+n}) \tag{20}$$

where $A_{m,n}(c,\zeta)$ is defined in (14).

We want to study spontaneous formation of clusters with rather small size polydispersity, or another words, inhomogeneity on a well-defined length scale $2\pi/k_0$. Such inhomogeneity can occur in the class of systems with the interaction potential V that in Fourier representation takes a deep negative minimum for $k=k_0>0$. When $\hat{V}(k_0)<0$, then the interactions favor oscillatory concentration, and the largest decrease of the energy takes place when the concentration wave with the wavenumber k_0 is excited (see (12)). Because of that, such concentration waves appear with a high probability, and in a given mesoscopic region with a linear size smaller than $2\pi/k_0$, the local concentration c is typically either larger or smaller than its average value. In such a case, the variance of the local concentration

$$\langle\phi^2\rangle=\int\frac{d\mathbf{k}}{(2\pi)^3}\hat{C}_{cc}^{-1}(k) \tag{21}$$

should be taken into account. However, local fluctuations of ζ are not energetically favored in this model, and $\langle\psi^2\rangle$ can be neglected.

Taking into account all the above assumptions, and using the property $\langle\phi(\mathbf{r}_1)^2\phi(\mathbf{r}_2)^2\rangle=2\langle\phi(\mathbf{r}_1)\phi(\mathbf{r}_2)\rangle^2$ of the Gaussian approximation, we obtain from (13) the following equations for $\mathbf{C}$ in Fourier representation

$$\hat{C}_{cc}(k)\approx\beta\hat{V}(k)+A_{0,2}+\frac{A_{0,4}}{2}\langle\phi^2\rangle-A_{1,2}^2\int d\mathbf{r}e^{i\mathbf{k}\cdot\mathbf{r}}G_{cc}(r)G_{\zeta\zeta}(r) \tag{22}$$

and

$$\hat{C}_{\zeta\zeta}(k)\approx A_{2,0}+\frac{A_{2,2}}{2}\langle\phi^2\rangle+\beta\hat{V}_{fl}(k), \tag{23}$$

where

$$\beta\hat{V}_{fl}(k)=-\frac{A_{1,2}^2}{2}\int d\mathbf{r}e^{i\mathbf{k}\cdot\mathbf{r}}G_{cc}(r)^2-\frac{A_{3,0}^2}{2}\int d\mathbf{r}e^{i\mathbf{k}\cdot\mathbf{r}}G_{\zeta\zeta}(r)^2. \tag{24}$$

Note that both, $\int d\mathbf{r}e^{i\mathbf{k}\cdot\mathbf{r}}G_{cc}(r)^2$ and $\int d\mathbf{r}e^{i\mathbf{k}\cdot\mathbf{r}}G_{\zeta\zeta}(r)^2$ are positive and even functions of k, and take a maximum for $k=0$. Thus, $\hat{V}_{fl}(k)$ induced by correlations between the fluctuations takes a negative minimum for $k=0$, and plays a role analogous to attractive interactions. For $k\to0$, Eq. (23) takes the form

$$\hat{C}_{\zeta\zeta}(k)=R_0+R_2k^2+\dots \tag{25}$$

where R_0,R_2 are given in Appendix. From Eq. (25), we obtain the asymptotic decay of correlations for large r in the real space

$$G_{\zeta\zeta}(r)=\frac{1}{4\pi R_2}\frac{\exp(-r/\xi_\zeta)}{r}. \tag{26}$$

where

$$\xi_\zeta=\sqrt{R_2/R_0}. \tag{27}$$

Let us return to C_{cc}. Because of the oscillatory decay of the concentration correlations, we expect that $\int d\mathbf{r}G_{cc}(r)G_{\zeta\zeta}(r)$ is small, and we assume that the last term in (22) can be neglected. With this assumption we obtain the Brazovskii-type approximation

$$\hat{C}_{cc}(k)\approx\beta\hat{V}(k)+A_{0,2}+\frac{A_{0,4}}{2}\int\frac{d\mathbf{k}}{(2\pi)^3}\hat{C}_{cc}^{-1}(k). \tag{28}$$

In this approximation, $\hat{C}_{cc}(k)$ is independent of the density–density correlations, and can be obtained for particular forms of $\hat{V}(k)$ by a self-consistent solution of Eq. (28). When $\hat{V}(k)$ is approximated by

$$\hat{V}(k)\approx\hat{V}(k_0)+v(k^2-k_0^2)^2+\dots, \tag{29}$$

valid for $k\approx k_0$, i.e. for the waves giving the largest decrease of the energy, then

$$\hat{C}_{cc}(k) \approx \hat{C}_{cc}(k_0) + \beta\nu(k^2 - k_0^2)^2 \tag{30}$$

where

$$\hat{C}_{cc}(k_0) \approx \beta\hat{V}(k_0) + A_{0,2} + \frac{A_{0,4}}{2}\int \frac{d\mathbf{k}}{(2\pi)^3}\hat{C}_{cc}^{-1}(k). \tag{31}$$

The analytical solution of (31) and (30) for $\hat{C}_{cc}(k_0)$ can be found easily, and the expression for $\hat{C}_{cc}(k_0)$ is given in Ref.[34]. The approximation (30) can lead to a fair accuracy of the last term in (31) only for $\hat{C}_{cc}(k)$ that has a high peak at $k = k_0$, so that the main contribution to the integral comes from the most probable wavenumbers. For this reason our analytical theory is valid only in systems with strong inhomogeneities, i.e. in a limited region of the phase diagram. In this approximation

$$G_{cc}(r) \approx \frac{A_{cc}\sin(k_0 r)\exp(-\alpha_0 r)}{r}, \tag{32}$$

with

$$A_{cc} \approx \langle\phi^2\rangle/k_0 \quad \text{and} \quad \alpha_0^{-1} \approx 8\pi\beta\nu\langle\phi^2\rangle. \tag{33}$$

Note that the amplitude and the correlation length of $G_{cc}(r)$ are proportional to the variance of the local concentration that for $\hat{C}_{cc}(k)$ approximated by (30) is given by

$$\langle\phi^2\rangle = \frac{k_0}{4\pi\sqrt{\beta\nu\hat{C}_{cc}(k_0)}}. \tag{34}$$

Once the form of $G_{cc}(r)$ is known, $\xi_\zeta = \sqrt{R_2/R_0}$ and R_2 can be obtained by a self-consistent solution of Eqs-(23)–(25). Explicit expressions are given in Appendix.

We have made a number of approximations, therefore we cannot expect full quantitative agreement of our final analytical expressions with simulations. In particular, the neglected last term in (22) would lead to a smaller value of $\tilde{C}_{cc}(k_0)$, and in turn to larger A_{cc} and $1/\alpha_0$ (see (33) and (34)). This in turn would lead to larger fluctuation-induced pseudo-interactions $|\hat{V}_{fl}(k)|$ and larger correlation length of the density–density correlations. When comparing our results with simulations, we should take into account that the correlations in the theory are underestimated. In the case of $\tilde{C}_{cc}(k)$, the fluctuation contribution is only a correction, while in the case of $\tilde{C}_{\zeta\zeta}(k)$, the whole k-dependence is induced by fluctuations. For this reason, the accuracy of our predictions for the density–density correlations is poorer than for G_{cc}.

Finally, we stress that in the MF approximation the density–density correlations are strictly local. We predict monotonic exponential decay of these correlations and show that their physical basis is the local fluctuation of the concentration.

3. Mesoscopic theory for binary mixtures near a planar wall

Here we develop the excess grand potential density functional in the semiinfinite system with the variance of the local densities taken into account. Our expression for the functional leads to highly simplified differential EL equations for the concentration and the volume fraction in inhomogeneous mixtures confined by a planar wall. Our equations can be solved analytically in a perturbation expansion.

3.1. Derivation of the excess grand potential functional in the mesoscopic theory

When a planar, homogeneous wall at $z = 0$ is present, translational invariance in the z-direction is broken, and external potentials $V_c(z)$ and $V_\zeta(z)$ appear. The average volume fraction and concentration differ from the bulk values, and vanish for $z < 0$. For $z > 0$, we introduce excess concentration and volume fraction,

$$c(\mathbf{r}_\parallel, z) = \bar{c} + \Delta c(\mathbf{r}_\parallel, z), \tag{35}$$

$$\zeta(\mathbf{r}_\parallel, z) = \bar{\zeta} + \Delta\zeta(\mathbf{r}_\parallel, z), \tag{36}$$

and in the following we limit ourselves to the disordered phase in the bulk with $\bar{\zeta} = const.$, $\bar{c} = 0$ and $\Delta c = c$.

The equilibrium c and $\Delta\zeta$ correspond to the minimum of the excess grand potential functional

$$\Delta\beta\Omega[c, \Delta\zeta] = \beta\Omega[c, \bar{\zeta} + \Delta\zeta] - \beta\Omega[0, \bar{\zeta}], \tag{37}$$

where $\Omega[c, \bar{\zeta} + \Delta\zeta]$ is the grand potential in the presence of the planar wall at $z = 0$, and $\Omega[0, \bar{\zeta}]$ is the grand potential in the same system in the absence of the wall. We expand $\Delta\beta\Omega$ in the functional Taylor series in c and $\Delta\zeta$. In the approximation consistent with our theory for the bulk, the second functional derivatives of $\beta\Omega$ contain fluctuation contributions and are given by (25) and (30), but the higher-order derivatives of $\beta\Omega$ are of the MF-type. Moreover, the first functional derivative of the grand potential vanishes at equilibrium. Thus, (37) takes the form

$$\Delta\beta\Omega[c, \Delta\zeta] = \Delta\beta\Omega_{2c}[c] + \Delta\beta\Omega_{2\zeta}[\Delta\zeta] + \int d\mathbf{r}_\parallel \int_0^\infty dz\big(\beta g_h(\bar{\zeta}, c, \Delta\zeta) + \beta V_c(z)c(\mathbf{r}_\parallel, z) + \beta V_\zeta(z)\zeta(\mathbf{r}_\parallel, z)\big) \tag{38}$$

where

$$\Delta\beta\Omega_{2c}[c] = \int \frac{d\mathbf{k}_\parallel}{(2\pi)^2}\int_0^\infty dz\,\tilde{c}(\mathbf{k}_\parallel, z)\int_0^\infty d\Delta z\tilde{C}_{cc}(k_\parallel, \Delta z)\,\tilde{c}(-\mathbf{k}_\parallel, z + \Delta z) \tag{39}$$

$$\Delta\beta\Omega_{2\zeta}[\Delta\zeta] = \int \frac{d\mathbf{k}_\parallel}{(2\pi)^2}\int_0^\infty dz\Delta\,\tilde{\zeta}(\mathbf{k}_\parallel, z)\int_0^\infty d\Delta z\tilde{C}_{\zeta\zeta}(k_\parallel, \Delta z)\Delta\,\tilde{\zeta}(-\mathbf{k}_\parallel, z + \Delta z) \tag{40}$$

and

$$\beta g_h(\bar{\zeta}, c, \Delta\zeta) = \sum_{m+n>2}\frac{A_{m,n}(0, \bar{\zeta})}{m!n!}\Delta\zeta^m c^n, \tag{41}$$

where $A_{m,n}$ is defined in (14). In (39) and (40), we use the Fourier representation in directions parallel to the wall and real-space representation in the z-direction, and tilde denotes the Fourier transform in the (x, y) plane.

In some thermodynamic states, a periodic, ordered structure can be formed in particle layers parallel to the substrate, and in such cases, $\Delta\zeta$ and c depend on $\mathbf{r}_\parallel$. In Ref. [7] such ordered patterns were observed in the gas phase when the transition to a crystal was approached. In this work we focus on thermodynamic states such that no periodic patterns in the plane (x, y) are expected, as for example seen in simulations of the one-component SALR system [8], where only short-range order at the wall was present. In this case, we assume that c and $\Delta\zeta$ depend only on z, and $\tilde{c}(\mathbf{k}_\parallel, z) = (2\pi)^2\delta(\mathbf{k}_\parallel)c(z)$, with analogous expression for $\Delta\tilde{\zeta}$. In order to simplify the calculations, we make an additional assumption of strictly short-range wall-particle interactions, $V_\alpha = h_\alpha\delta(z)$, and obtain

$$\Delta\beta\Omega[c, \Delta\zeta]/A = \beta\Omega_{2c}[c]/A + \beta\Omega_{2\zeta}[\Delta\zeta]/A + \int_0^\infty dz\beta g_h + \beta h_c c(0) + \beta h_\zeta\zeta(0) \tag{42}$$

where A denotes the surface area, and

$$\beta\Omega_{2c}[c]/A = \int_0^\infty dz c(z)\int_0^\infty d\Delta z\tilde{C}_{cc}(0, \Delta z)c(z + \Delta z), \tag{43}$$

with analogous formula for $\beta\Omega_{2\zeta}$.

In order to develop a functional of the Landau-Brazovskii type for which the EL equations are particularly simple, we consider

the even and the odd powers of Δz in the Taylor expansion of $c(z+\Delta z)$ in (43) separately, and focus on the formula

$$\int_0^\infty d\Delta z \tilde{C}_{cc}(0,\Delta z)c(z+\Delta z) = E_c(z) + O_c(z). \tag{44}$$

For the sum of the even powers of Δz we obtain

$$\begin{aligned} E_c(z) &= \int_0^\infty d\Delta z \tilde{C}_{cc}(0,\Delta z)\sum_{n=0}^\infty \frac{\Delta z^{2n}}{(2n)!}\frac{d^{2n}}{dz^{2n}}c(z) \\ &= \tfrac{1}{2}\int_{-\infty}^\infty d\Delta z \tilde{C}_{cc}(0,\Delta z)\exp\left(i\Delta z\left(-i\tfrac{d}{dz}\right)\right)c(z) \\ &= \tfrac{1}{2}\hat{C}_{cc}\left(-i\tfrac{d}{dz}\right)c(z), \end{aligned} \tag{45}$$

where a function of a differential operator is defined by the Taylor expansion, we used the symmetry $\tilde{C}_{cc}(0,\Delta z) = \tilde{C}_{cc}(0,-\Delta z)$ and the fact that the integral of an odd function vanishes. The sum of the odd powers is

$$O_c(z) = \sum_{n=0}^\infty \int_0^\infty d\Delta z \tilde{C}_{cc}(0,\Delta z)\frac{\Delta z^{2n+1}}{(2n+1)!}\frac{d^{2n+1}}{dz^{2n+1}}c(z). \tag{46}$$

Note that by inserting (46) into (43), we obtain a sum of terms proportional to $\int_0^\infty dz c(z) d^{2n+1}c(z)/dz^{2n+1}$. By integrating by parts the above integrals, we obtain a contribution to Ω_{2c}/A localized at the surface, i.e. depending only on $c(0)$ and its derivatives. The same considerations can be applied to $\beta\Omega_{2\zeta}/A$, defined by an equation analogous to (43).

The sum of the even powers of Δz in the expansions of $c(z+\Delta z)$ and $\Delta\zeta(z+\Delta z)$ gives the bulk contributions, and for $C_{\alpha\alpha}$ approximated by (25) and (30), $\Delta\beta\Omega$ takes the form

$$\begin{aligned} \Delta\beta\Omega[c,\Delta\zeta]/A &= \frac{1}{2}\int_0^\infty dz c(z)\left(A_4\frac{\partial^4}{\partial z^4} + A_2\frac{\partial^2}{\partial z^2} + A_0\right)c(z) \\ &+ \frac{1}{2}\int_0^\infty dz \Delta\zeta(z)\left(R_0 - R_2\frac{d^2}{dz^2}\right)\Delta\zeta(z) + \int_0^\infty dz \beta g_h + \beta u_I, \end{aligned} \tag{47}$$

where βg_h is defined in (41) and

$$A_0 = \hat{C}_{cc}(k_0) + \beta\nu k_0^4 \tag{48}$$

$$A_2 = 2\beta\nu k_0^2 \tag{49}$$

$$A_4 = \beta\nu. \tag{50}$$

To obtain the surface contribution βu_I in the functional (47), we truncate the Taylor expansion of $c(z+\Delta z)$ in the odd powers of Δz in (43) at the term consistent with the fourth-order derivative of c in the first term in (47). Since in the second term in (47) only the second-order derivative of $\Delta\zeta$ is present, the Taylor expansion of $\Delta\zeta(z+\Delta z)$ in the odd powers of Δz is truncated at the first-order term. The result is

$$\begin{aligned} \beta u_I &= \beta h_c c(0) + \beta h_\zeta \zeta(0) - \frac{1}{2}\left(O_1^c c(0)^2 + O_1^\zeta \Delta\zeta(0)^2\right) \\ &- O_3^c c(0)c''(0) + \frac{O_3^c}{2}|c'(0)|^2 \end{aligned} \tag{51}$$

with

$$O_{2n+1}^\alpha = \int_0^\infty d\Delta z \tilde{C}_{\alpha\alpha}(0,\Delta z)\frac{\Delta z^{2n+1}}{(2n+1)!}. \tag{52}$$

The first two terms in (51) represent the wall-fluid interactions. The contribution to $\Delta\beta\Omega$ coming from the missing fluid particles for $z<0$ is compensated by the remaining terms.

3.2. The Euler–Lagrange equations

By the minimization of the functional (47) and (51) we easily obtain the EL equations

$$\left(A_0 + A_2\frac{d^2}{dz^2} + A_4\frac{d^4}{dz^4}\right)c(z) + \frac{\partial\beta g_h(\bar{\zeta},c(z),\Delta\zeta(z))}{\partial c(z)} = 0 \tag{53}$$

$$\left(R_0 - R_2\frac{d^2}{dz^2}\right)\Delta\zeta(z) + \frac{\partial\beta g_h(\bar{\zeta},c(z),\Delta\zeta(z))}{\partial\Delta\zeta(z)} = 0 \tag{54}$$

and the boundary conditions,

$$\frac{\beta\nu}{2}c'''(0) - \beta O_3^c c''(0) + \beta\nu k_0^2 c'(0) - \beta O_1^c c(0) + \beta h_c = 0 \tag{55}$$

$$\frac{\beta\nu}{2}c''(0) - \beta O_3^c c'(0) + \beta\nu k_0^2 c(0) = 0 \tag{56}$$

$$-\frac{R_2}{2}\Delta\zeta'(0) - \beta O_1^\zeta \Delta\zeta(0) + \beta h_\zeta = 0 \tag{57}$$

3.3. Approximate analytical solutions of the EL equations

For large z we can solve linearized Eqs. 53,54, because both $c(z)$ and $\Delta\zeta(z)$ are small for $z\to\infty$. The second term in (53) and (54) is of a second order in the fields c and $\Delta\zeta$, therefore only the first terms remain and the linearized equations are decoupled. The solutions are

$$\Delta\zeta^{(0)}(z) = A_\zeta^0 e^{-z/\xi_\zeta} \tag{58}$$

and

$$c^{(0)}(z) = A_c e^{-\alpha_0 z}\sin(k_0 z + \theta) \tag{59}$$

with ξ_ζ and α_0 given in (27) and (33), respectively. The amplitudes are proportional to the contact potentials h_ζ and h_c . In addition, A_ζ^0 and A_c as well as the phase depend on the interactions, in particular on the semimoments (52), and on the thermodynamic state.

Now, in the perturbation expansion, we truncate the series for $\beta g_h(\bar{\zeta},c,\Delta\zeta)$ at $m=1,n=2$ (see (41)) and approximate the EL Eqs. 53,54 by

$$\left(-R_2\frac{\partial^2}{\partial z^2} + R_0\right)\Delta\zeta(z) + \frac{A_{1,2}}{2}c^{(0)}(z)^2 = 0, \tag{60}$$

$$\left(A_4\frac{\partial^4}{\partial z^4} + A_2\frac{\partial^2}{\partial z^2} + A_0\right)c(z) + A_{1,2}\Delta\zeta^{(0)}(z)c^{(0)}(z) = 0. \tag{61}$$

The solutions of the above equations are sums of the solution of the linear equation and a correction. Note that the correction term in (61) decays faster than the solution of the linear equation. However, the correction term in (60) can have a longer range than the solution of the linear equation, if $2\alpha_0 < 1/\xi_\zeta$. We conclude that the asymptotic decay of $c(z)$ is correctly predicted by the linear equation. For $\Delta\zeta$ we solve (60) and obtain

$$\Delta\zeta(z) = A_\zeta e^{-z/\xi_\zeta} + f(z)e^{-2\alpha_0 z} \tag{62}$$

with

$$f(z) = A_p\cos(2k_0 z + \theta_1) + A_m, \tag{63}$$

where θ_1, A_ζ, A_p, and A_m depend on the thermodynamic state and on the particle–particle and the particle–wall interactions. The rather lengthy formulas are not given here. We stress that the EL equations are strongly nonlinear, and the above approximation is in principle valid only for weak wall-particle interactions and far from any

phase transitions. Moreover, in the coarse-grained theory with the local-density approximation for the hard-sphere reference system, the density at short distances from the wall cannot be correctly predicted.

The adsorption in this approximation takes the form

$$\Gamma = \int_0^\infty dz\Delta\zeta(z) = A_\zeta\xi_\zeta + \frac{A_m}{2\alpha_0} + A_p\frac{\alpha_0\cos\theta_1 - k_0\sin\theta_1}{2(\alpha_0^2+k_0^2)}, \tag{64}$$

and the selective adsorption is

$$\Gamma_s = \int_0^\infty dzc(z) = A_c\frac{\alpha_0\cos\theta - k_0\sin\theta}{\alpha_0^2+k_0^2}. \tag{65}$$

We can see that the total adsorption increases with increasing correlation lengths ξ_ζ and $1/\alpha_0$. The selective adsorption, however, is bounded by $|\Gamma_s| \leqslant A_c/k_0$ for $\alpha_0 \to 0$. This means that in the adsorbed film the amount of the particles of each type is comparable. This result agrees with simulations [7].

4. Results for a representative model

In order to model a mixture of oppositely charged hydrophilic and hydrophobic particles in near-critical solvents, we choose the double Yukawa potential between like particles, $u_{ii} = -u_{ij} = u$, with

$$u(r) = -K_1\frac{\exp(-\kappa_1 r)}{r} + K_2\frac{\exp(-\kappa_2 r)}{r}, \tag{66}$$

where $K_1 = 1, K_2 = 0.2, \kappa_1 = 1$ and $\kappa_2 = 0.5$. This potential belongs to the SALR-type interaction potentials, and leads to a formation of rather large clusters. As noted in Section 2, in order to avoid contributions to the internal energy coming from overlapping cores of the particles and to rescale the potential due to the replacement of the density by the volume fraction in Eq. (12), we assume $V(r) = u(r)\theta(r-1)(6/\pi)^2$ in our theoretical formulas. We shall consider the volume fraction of all particles, ζ, and the dimensionless temperature $T^* = k_BT/K_1$ as thermodynamic variables.

The theoretical results for this model are presented in Section 4.1 and compared with results of MC simulations in Section 4.2.

4.1. Theoretical results

In this model, the parameters present in the approximation (29) for $\hat{V}(k)$ take the values: $k_0 \simeq 0.6088, \hat{V}(k_0) \simeq -10.092, \nu \simeq 20.563$. For the reference system free-energy associated with close-packing (see (11)) we assume the CS approximation [33]

$$\beta f_{ex}(\zeta) = \rho\left[\frac{4\zeta - 3\zeta^2}{(1-\zeta)^2} - 1\right]. \tag{67}$$

The correlation lengths of the concentration-concentration and density–density correlation functions are shown in Fig. 1 for a range of $\bar{\zeta}$ at two fixed temperatures, $T^* = 0.25$ and $T^* = 0.28$. We can see that both correlation lengths increase significantly with increasing volume fraction. While the increase of $1/\alpha_0$ is gradual (almost linear), ξ_ζ increases very slowly for small ζ, and next at the volume fraction increasing with increasing T^*, a rapid growth of ξ_ζ begins. The concentration-concentration correlation function in Fourier representation is shown in Fig. 2. We can see a maximum increasing with increasing $\bar{\zeta}$, signaling stronger inhomogeneities and better accuracy of our approximate theory for larger density.

Let us focus on the near-surface structure. The phases θ and θ_1 of the concentration and volume-fraction profiles (see (59) and (62)–(63)) depend on the interparticle interactions and thermodynamic state, whereas the amplitudes A_c and A_ζ^0 depend in addition on the surface-fluid interactions h_c and h_ζ, respectively. We assume $h_c = h_\zeta$ to model a surface attracting only the first component. We tune h_c such that $A_c = 0.5$. The obtained $c(z)$ and $\Delta\zeta(z)$ are shown in Fig. 3 for $T^* = 0.28$ and $\bar{\zeta} = 0.065, 0.07$, i.e. for rather small volume fractions and as seen in Fig. 1, rather small correlation lengths. The oscillatory decay of $\Delta\zeta(z)$ superimposed on the monotonic decay can be clearly seen. Thus, the asymptotic decay of the density at large distances from a wall cannot be deduced solely from the decay of the density–density correlations in the bulk. It depends on the concentration-concentration correlations in the bulk too.

The adsorption Γ, Eq. (64), describes the excess of the number of particles per unit area σ^2 of the wall. In Fig. 4, Γ is shown for the surface attracting the first component. As expected, the adsorbed amount of particles increases with increasing bulk density.

4.2. Results of MC simulations

To verify the theoretical predictions, we performed MC simulations in the μVT ensemble. Particles of the same diameter ($\sigma_1 = \sigma_2 = \sigma = 1.0$) interacted with the SALR potential beyond the hard cores, with $u_{ii} = -u_{ij} = u$, and with u given in Eq. (66). The cut-off radius was 15 σ. The same chemical potentials of the two species were assumed, $\mu_1 = \mu_2$ [24,25]. First, we simulated the bulk symmetrical binary mixture to be used as a reference system. The particles were placed in a cubic box of edge length 60 σ with periodic boundary conditions applied to the system in the three directions. Each system has run 10^6 MC steps for equilibration and 10^5 for production. Because of the inhomogeneities on the length scale 10σ, finite size effects may have some impact on the correlation functions. However, for verification of the theory on the qualitative or semiquantitative level, we do not need very good quantitative accuracy for the correlation functions in the bulk.

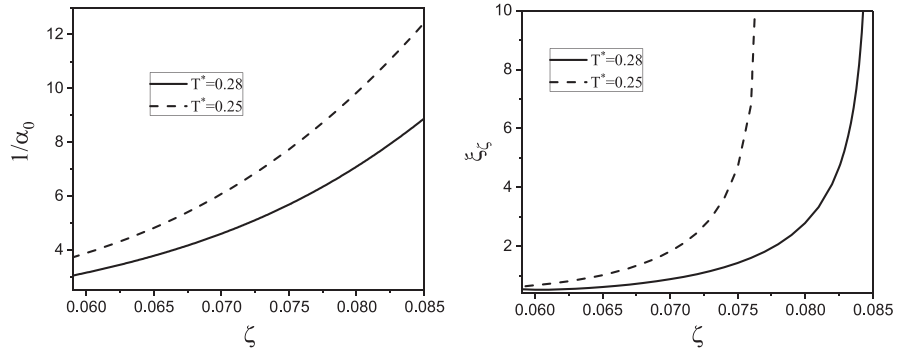

Fig. 1. The decay length $\alpha_0^{-1}(\zeta)$ of the concentration-concentration correlation function (32) (left panel) and the decay length ξ_ζ of the density–density correlation function (right panel) for the double Yukawa potential (66) as a function of the volume fraction of particles ζ for $T^* = 0.25$ and $T^* = 0.28$.

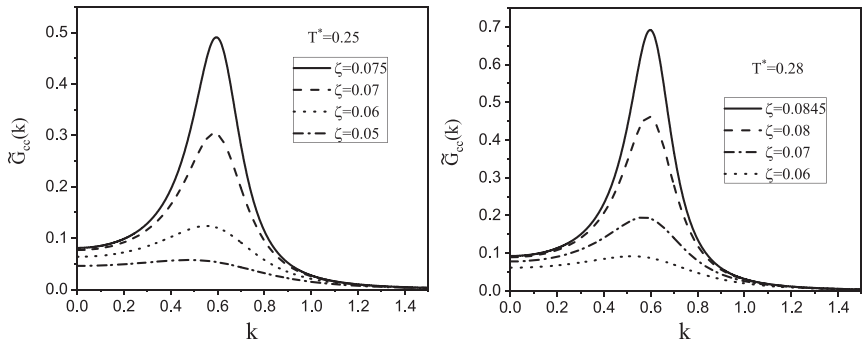

Fig. 2. The concentration-concentration correlation functions (32) in Fourier representation for $T^* = 0.25$ (left panel) and $T^* = 0.28$ (right panel) for the double Yukawa potential (66) and the volume fractions indicated in the legends.

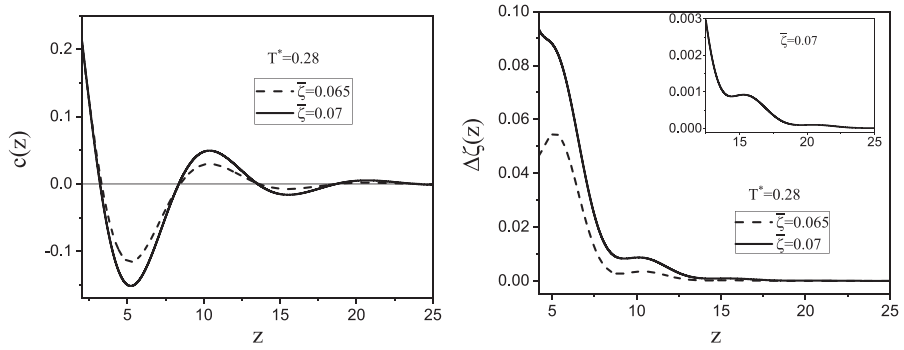

Fig. 3. The concentration (59) (left panel) and the volume fraction (62) (right panel) for the double Yukawa potential (66) as functions of the distance z from the attractive wall for $\bar{\zeta} = 0.065, 0.07$ and $T^* = 0.28$. The amplitude is fixed to $A_c = 0.5$ that corresponds to the particle–wall interaction $h_c = h_\zeta = -19.69, -18.60$ for $\bar{\zeta} = 0.065, 0.07$, respectively. Inset: the behaviour of $\Delta\zeta(z)$ for $z > 12$ ($\bar{\zeta} = 0.07$).

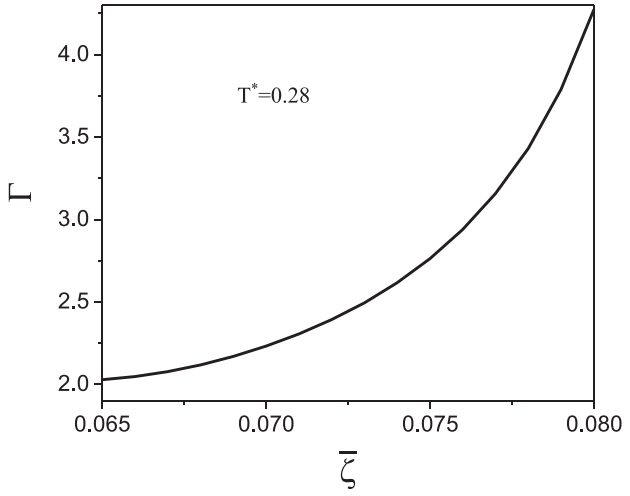

Fig. 4. The adsorption (64) for the double Yukawa potential (66) as a function of the bulk volume fraction of the particles at $T^* = 0.28$ and for the particle–wall interaction $h_c = h_\zeta = -20$.

In order to simulate this symmetrical binary mixture confined in a semi-infinite system, we assume that there is a homogeneous planar wall of width 16σ centered at $z = 0$, (xy plane). In addition to the steric interactions of the particles of the two species with the wall, we assume that the particles of the first species interact with the wall with the attractive potential $v_w(z) = -A_w \exp(-k_w z)$, with $A_w = 1.0$ and $k_w = 2.0$. As the wall is in the center of the box, the periodic boundary conditions are applied to the system in the three directions, with $L_x = L_y = 40\sigma$. L_z has been enlarged till $\zeta_1(z)$ and $\zeta_2(z)$ reached the bulk value for $z \approx L_z/2$. We found that $L_z = 100\sigma$ was sufficiently large to mimic a semi-infinite system.

The concentration $c(z)$ and the excess volume fraction $\Delta\zeta(z)$ obtained in the MC simulations for $T^* = 0.28$ and $\bar{\zeta} = 0.051$ are shown in Fig. 5 together with the best fits to Eqs. (59) and (62)–(63), respectively. The parameters A_c and θ for $c(z)$, and A_ζ, A_p, A_m and θ_1 for $\Delta\zeta(z)$, were fitted to the simulation results. The decay lengths ξ_ζ and $1/\alpha_0$ and the wave number k_0 were fitted to the simulation results for $c(z)$ and $\Delta\zeta(z)$, as well as to the simulation results for the two correlation functions. The correlation functions with the fits to Eqs. (32) and (26) are shown in the insets in Fig. 5. The oscillatory decay of $G_{cc}(r)$ and the monotonic decay of $G_{\zeta\zeta}(r)$ agree with our theoretical predictions. The wavenumber of the oscillatory decay of the concentration-concentration correlation function obtained in simulations is very close to our theoretical prediction $k_0 \approx 0.6088$ obtained from the minimum of $\hat{V}(k)$. This confirms that the length scale of inhomogeneity is determined by the interaction potential, and therefore it is correctly predicted even in the MF approximation. In contrast, the decay lengths and the amplitudes of the correlation functions depend on the way the fluctuations of the local concentration are taken into account. As discussed in Section 2, the correlations in our analytical theory are underestimated, and the results for the parameters α_0, ξ_ζ and A_{cc}, R_2 are correct on the semi-quantitative level only. The formulas (32) and (26), however, describe rather well the simulation results for $z > 7$ when the above parameters are fitted.

The formula (59) for the concentration profile obtained from the linearized EL equation reproduces the simulation results with quite

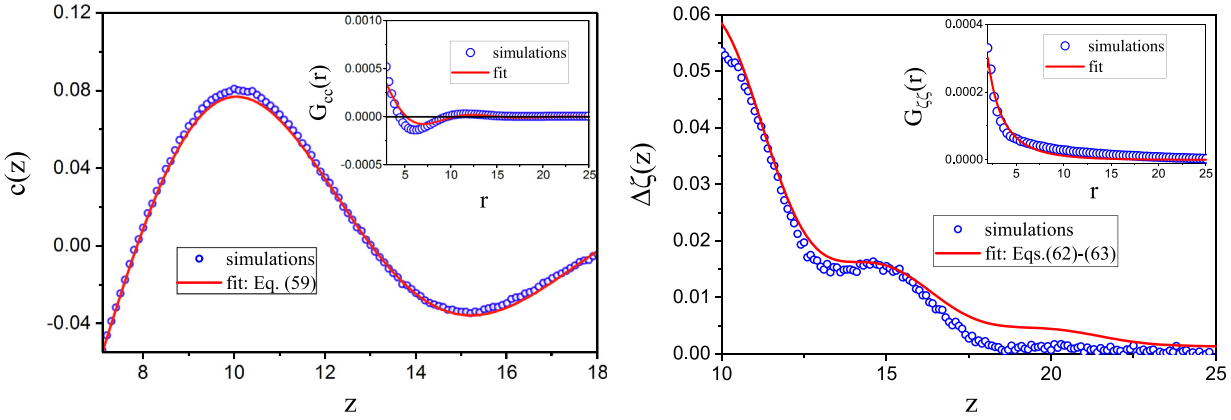

Fig. 5. The concentration $c(z)$ (left) and the excess volume fraction $\Delta\zeta(z) = \zeta(z) - \bar{\zeta}$ (right panel) for $T^* = 0.28$ and $\bar{\zeta} = 0.051$ for the double Yukawa potential (66), as functions of the distance z from the attractive wall. In the insets, the correlation functions in the bulk are shown. The results of the MC simulations are shown by the symbols. The fits of the simulation data to Eqs. (32), (26), (59) and (62)–(63) are shown by the solid lines. In all the plots, $\alpha_0 = 0.148, k_0 = 0.609$ and $\xi_\zeta = 4.896$. The remaining parameters are $A_{cc} = 0.006, 1/(4\pi R_2) = 0.0033$, for $G_{cc}(r)$ and $G_{\zeta\zeta}(r)$ respectively, $A_c = 0.35$ and $\theta = 1.493$ for $c(z)$, and $A_\zeta = 0.153, A_m = 0.56, A_p = 0.22$ and $\theta_1 = -0.186$ for $\Delta\zeta(z)$. z is in units of the molecular diameter.

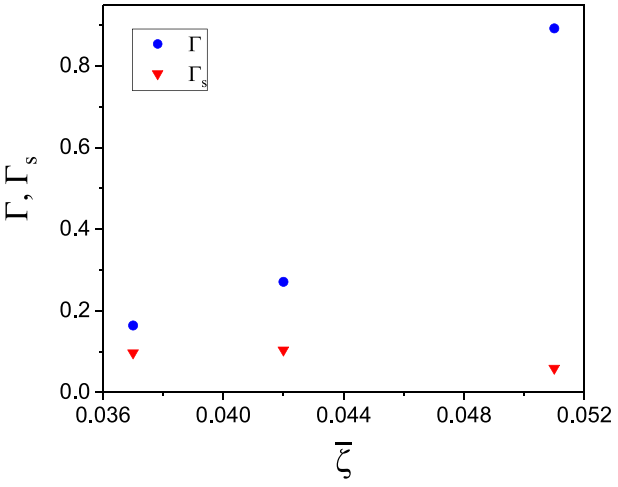

Fig. 6. Simulation results for the adsorption (circles) and the selective adsorption (triangles) per unit area of the surface, $\Gamma(\bar{\zeta})$ and $\Gamma_s(\bar{\zeta})$ defined in Eq. (64) and (65), respectively for $T^* = 0.28$.

good accuracy. For the density, however, the linear approximation (Eq. (58)) fails completely, because instead of the predicted exponential decay, oscillations superimposed on the monotonic decay are present. A fair agreement between the simulations and the formula (62)–(63) is obtained beyond the linear approximation, at the first order in the perturbation expansion. Both the simulations and the theory show the oscillatory decay superimposed on the monotonic decay, with the maxima of $\Delta\zeta(z)$ at the same distances from the wall in the two cases. Thus, our prediction that the wavenumber of the density oscillations is twice the wavenumber of the oscillations of the concentration-concentration correlation function is quantitatively correct. However, the amplitude of the oscillations is underestimated in the formula (62)–(63).

The simulation results (Fig. 5) can be compared with our theoretical predictions obtained for $T^* = 0.28, \bar{\zeta} = 0.07$ and the contact potential $h_c = h_\zeta = -18.60$ (Fig. 3). The concentration profiles in the theory and simulations are very similar, and the extrema of $\Delta\zeta(z)$ are at very similar distances from the wall. The magnitude of $\Delta\zeta(z)$ in Fig. 3 is underestimated, however, mostly because of the underestimated amplitudes. We should stress that the only adjusted parameter in Fig. 3 is the contact potential $h_c = h_\zeta$ that mimics the exponentially decaying attraction in the simulations. Besides that, no more parameters were fitted.

Fig. 5 shows that the functions predicted by our theory reproduce quite well the shapes of $c(z)$ and $\Delta\zeta(z)$ also beyond the range of validity of our perturbation expansion, valid for very weak wall-particle interaction. The parameters in our equations, especially the amplitudes, are not sufficiently accurate for strongly attractive surfaces, as can be seen from the comparison of Figs. 5 and 3.

The adsorption computed for $\bar{\zeta} \leqslant 0.051$ and shown in Fig. 6 has a shape similar to our theoretical result shown in Fig. 4. We calculated Γ for $\bar{\zeta} \geqslant 0.065$, because our analytical theory is not valid for smaller densities. We can see, however that the magnitude of Γ is similar in the theory and simulations, and the selective adsorption is small, in agreement with our predictions.

The simulation results give additional insight into the structure in the layers parallel to the wall. A snapshot of the equilibrium structure in half of the simulation box is shown in Fig. 7 for $T^* = 0.28$ and $\mu_1 = \mu_2 = -0.839$. In addition to the side view, we show particles in layers of thickness 2 parallel to the wall, at four distances from it.

In the regions around the maxima of $\rho_i(z)$ (see Fig. 7 (f)), one can recognize the structure found in the two dimensional SALR model at a similar average density [4], i.e. bubbles for $0 < z < 2$ (Fig. 7 b), stripes for $4 < z < 6$ (Fig. 7 d) and clusters for $9 < z < 11$ (Fig. 7 e), all with the linear size $\pi/k_0 \approx 5$. Between the layers rich in the first and the second component, i.e. around the minima of $\Delta\zeta(z)$, neighboring clusters of the two components and small voids are formed (Fig. 7c). When z increases, the clusters in the layers with comparable amount of the two components become less compact.

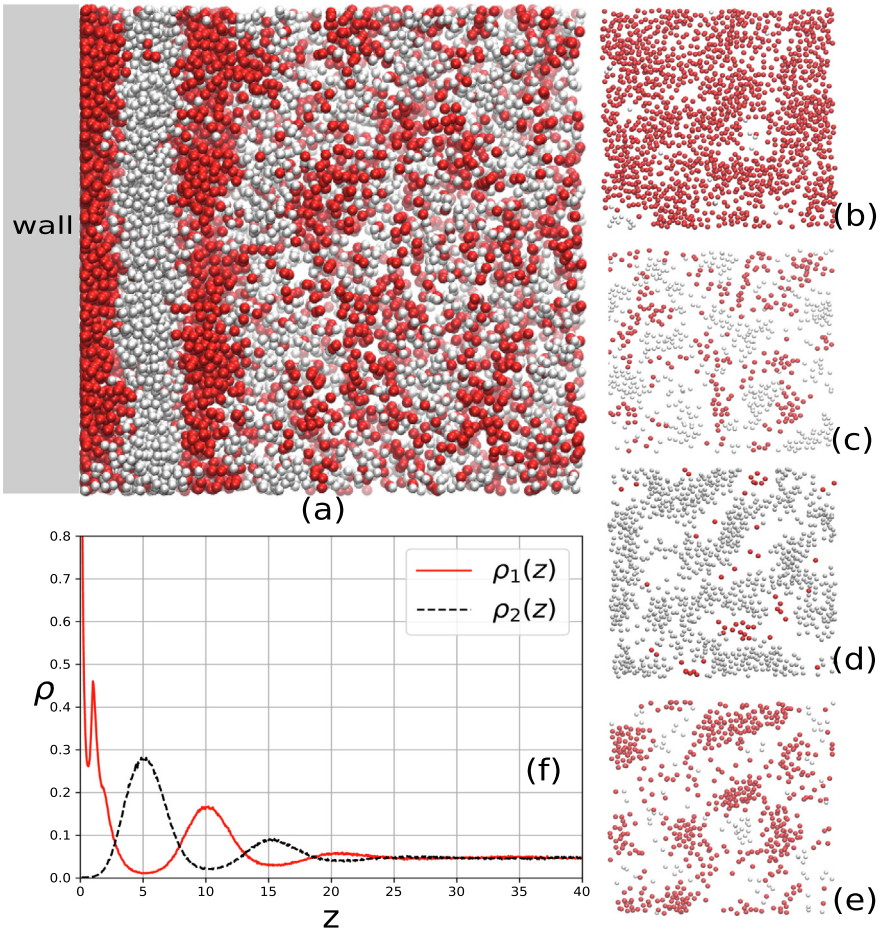

Fig. 7. Snapshot of half of the simulation box, $z > 0$. (a): side view of the simulated binary mixture in contact with a wall (grey region in the left part of the figure). $T^* = 0.28, \mu_1 = \mu_2 = -0.839, L_x = L_y = 40\sigma$ and $L_z = 100\sigma$. (b)-(e): snapshots of layers of a width 2σ parallel to the wall, with $0 \leqslant z \leqslant 2$ (b), $2 \leqslant z \leqslant 4$ (c), $4 \leqslant z \leqslant 6$ (d) and $9 \leqslant z \leqslant 11$ (e). (f): a density profile as a function of z of each component of the mixture.

5. Conclusions

We studied the effect of a planar wall on a symmetrical binary mixture with interactions leading to spontaneous inhomogeneities on a well defined length scale. We assumed that the interactions outside the hard cores of the particles of the i-th and j-th components are $u_{ii} = -u_{ij} = u$, with u having the SALR form. This type of interactions favors concentration waves with a well-defined wavenumber, but the density waves are not energetically favorable, therefore no long-range correlations between density fluctuations, as well as no excess density at large distances from the wall can be obtained in the MF approximation.

The main result of our work is the approximation for the excess grand potential functional of the concentration and the excess volume fraction, Eqs. (47) and (51).The functional has a form of a sum of the Brazovskii-functional [32] of the concentration, the Landau-functional of the excess volume fraction, and a cross-term where the two order parameters are coupled. In our theory, the role of attractive interactions in the functional (47) is played by the correlations between fluctuations of the local concentration.

The Euler–Lagrange Eqs. 53,54 derived from the functional (47) are simple differential equations and can be solved analytically in the perturbation expansion. The concentration and excess volume fraction profiles are given by (59) and (62)–(63) respectively. The characteristic lengths of the concentration profile are entirely determined by the concentration-concentration correlation function. The decay of $\Delta\zeta(z)$, however, depends on both, the density–density and concentration-concentration correlation functions.

Our theory was applied to a model with the double Yukawa interactions (66), and the results were verified by Monte Carlo simulations. The functional form of the correlation functions is in a good agreement with the simulations - the concentration-concentration correlations show oscillatory decay, and the density–density correlations decay monotonically. The concentration profile (59) agrees very well with simulations already for z larger than the period of oscillations, as found previously for different systems [8,18]. Also the prediction that $\Delta\zeta(z)$ is a sum of a monotonic and an oscillatory decay was confirmed by simulations. We verified that the period of oscillations is half the period of the concentration-concentration correlation function. The perturbation expansion in our analytical theory is in principle valid only for weak wall-particle interactions. Still, a semiquantitative agreement with simulations is obtained also for rather strong $h_c = h_\zeta$.

We conclude that the predicted expressions for the concentration and excess volume fraction correctly describe the near-surface structure, with good quantitative agreement in the case of concentration, and semiquantitative agreement in the case of excess volume fraction. The predicted dependence of the parameters in Eqs. (59) and (62)-(63) on the thermodynamic state and the interparticle interactions, however, is less accurate because of the approximations done in order to obtain analytical expressions.

While in the one component SALR systems the adsorption decreases with increasing density when the clusters dominate, in the symmetrical mixture the adsorption increases with increasing density. In the adsorbed film, the amount of particles of the two components is comparable, even when only the first component is attracted to the wall.

Simulations show that in the layers parallel to the wall that are rich in one of the two components, the structure closely resembles the structure found previously for the two-dimensional SALR systems with similar average density. In the layers parallel to the wall centered at the extrema of $c(z)$, we see bubbles, stripes and clusters for increasing distance from the wall (Fig. 7). These almost one-component layers are separated by layers with comparable amount of the two components, with clusters of different particles being close neighbors, as in the bulk. We conclude that an external surface significantly enhances ordering of the mixture, and leads to a sequence of different patterns in its neighborhood.

Declaration of Competing Interest

The authors declare that they have no known competing financial interests or personal relationships that could have appeared to influence the work reported in this paper.

Acknowledgments

This work was supported by the European Union Horizon 2020 research and innovation programmes under the Marie Skłodowska-Curie grant agreement No. 734276. (CONIN) Additional funding was received from the Polish Ministry of Science and Higher Education for the implementation of the project No. 734276 in the years 2017–2022.

Appendix A. Expressions for the parameters R_0 and R_2

From (23)–(25) we obtain the following expressions for the parameters R_0 and R_2,

$$R_0 = A_{2,0} + \frac{A_{2,2}}{2}\langle\phi^2\rangle - 4\pi\left(\frac{A_{1,2}^2}{2}\int_0^\infty drr^2 G_{cc}(r)^2 + \frac{A_{3,0}^2}{2}\int_0^\infty drr^2 G_{\zeta\zeta}(r)^2\right) \tag{68}$$

and

$$R_2 = \frac{4\pi}{3!}\left(\frac{A_{1,2}^2}{2}\int_0^\infty drr^4 G_{cc}(r)^2 + \frac{A_{3,0}^2}{2}\int_0^\infty drr^4 G_{\zeta\zeta}(r)^2\right). \tag{69}$$

For $G_{cc}(r)$ and $G_{\zeta\zeta}$ given in (32) and (26), the explicit forms of $\xi_\zeta = \sqrt{R_2/R_0}$ and R_2 are obtained by the solution of the equations

$$\frac{R_2}{\xi_\zeta^2} = A_{2,0} + \frac{A_{2,2}}{2}\langle\phi^2\rangle - \left(\frac{A_{1,2}^2}{2}\frac{\pi A_{cc}^2 k_0^2}{\alpha_0(\alpha_0^2+k_0^2)} + \frac{A_{3,0}^2}{2}\frac{\xi_\zeta}{8\pi R_2^2}\right) \tag{70}$$

and

$$R_2 = \frac{4\pi}{3!}\left(\frac{A_{1,2}^2}{2}\frac{A_{cc}^2 k_0^2(6\alpha_0^4 + 3k_0^2\alpha_0^2 + k_0^4)}{8\alpha_0^3(\alpha_0^2+k_0^2)^3} + \frac{A_{3,0}^2}{2}\frac{\xi_\zeta^3}{4(4\pi R_2)^2}\right). \tag{71}$$

where $A_{m,n}, A_{cc}$ and α_0 are given in (14) and (33), and $\langle\phi^2\rangle$ is given in (34).

References

[1] D. Antelmi, P. Kékicheff, P. Richetti, J. Phys. II France 5 (1995) 103.
[2] B. Yu, P. Sun, T. Chen, Q. Jin, D. Ding, B. Li, A.-C. Shi, Phys. Rev. Lett. 96 (2006) 138306.
[3] A. Imperio, L. Reatto, Phys. Rev. E 76 (2007) 040402.
[4] A.J. Archer, Phys. Rev. E 78 (2008) 031402.
[5] P. Chi, Z. Wang, B. Li, A.-C. Shi, Langmuir 27 (2011) 11683.
[6] C. Bores, N. Almarza, E. Lomba, G. Kahl, J. Phys.: Condens. Matter 27 (2015) 194127.
[7] M. Litniewski, A. Ciach, Molecules 26 (2021) 4532.
[8] M. Litniewski, A. Ciach, J. Chem. Phys. 150 (2019) 234702.
[9] V.V.E. Bildanau, J. Pękalski, A. Ciach, Phys. Rev. E 101 (2020) 012801.
[10] N.G. Almarza, J. Pękalski, A. Ciach, Soft Matter 12 (2016) 7551.
[11] J. Pękalski, E. Bildanau, A. Ciach, Soft Matter 15 (2019) 7715.
[12] H. Serna, W.T. Gozdz, E.G. Noya, Langmuir 35 (2019) 702.
[13] H. Serna, E.G. Noya, W.T. Gozdz, Soft Matter 16 (2020) 718.
[14] K. Marolt, R. Roth, Phys. Rev. E 102 (2020) 042608.
[15] A. Stradner, H. Sedgwick, F. Cardinaux, W. Poon, S. Egelhaaf, P. Schurtenberger, Nature 432 (2004) 492.
[16] A.P. Santos, J. Pękalski, A.Z. Panagiotopoulos, Soft Matter 13 (2017) 8055.
[17] A. Ciach, Phys. Rev. E 100 (2019) 062607.
[18] J.M. Otero-Mato, H. Montes-Campos, O. Cabeza, D. Diddens, A. Ciach, L.J. Gallego, L.M. Varela, Phys. Chem. Chem. Phys. 20 (2018) 30412.
[19] R. Evans, Adv. Phys. 28 (1979) 143.
[20] R. Evans, M. Oettel, R. Roth, G. Kahl, J. Phys.: Condens. Matter 28 (2016) 240401.
[21] H.W. Diehl, Field-theoretic Approach to Critical Behavior at Surfaces, Phase Transitions and Critical, in: Phenomena, 1st ed., 10, Academic Press, London, 1986, pp. 75–267.
[22] C.A. Ferreiro-Rangel, M.B. Sweatman, Mol. Phys 116 (21–22) (2018) 3231.
[23] J. Tan, N.D. Afify, C.A. Ferreiro-Rangel, X. Fan, M.B. Sweatman, J. Chem. Phys. 154 (2021) 074504.
[24] O. Patsahan, M. Litniewski, A. Ciach, Soft Matter 17 (2021) 2883.
[25] A. Ciach, O. Patsahan, A. Meyra, Condens. Matter Phys. 23 (2020) 23601.
[26] G. Munao, S. Prestipino, J.-M. Bomont, D. Costa, J. Phys. Chem. B 126 (2022) 2027.
[27] C. Hertlein, L. Helden, A. Gambassi, S. Dietrich, C. Bechinger, Nature 451 (2008) 172.
[28] A. Gambassi, A. Maciołek, C. Hertlein, U. Nellen, L. Helden, C. Bechinger, S. Dietrich, Phys. Rev. E 80 (2009) 061143.
[29] U. Nellen, J. Dietrich, L. Helden, S. Chodankar, K. Nygard, J.F. van der Veen, C. Bechinger, Soft Matter 80 (2011) 061143.
[30] A. Ciach, J. Pękalski, W.T. Góźdź, Soft Matter 9 (2013) 6301.
[31] A. Ciach, Mol. Phys 109 (2011) 1101.
[32] S.A. Brazovskii, Sov. Phys. JETP 41 (1975) 85.
[33] N.F. Carnhan, K.E. Starling, J. Chem. Phys. 51 (1969) 635.
[34] A. Ciach, O. Patsahan, Condens. Matter Phys. 15 (2012) 23604.